Eur. J. Mineral.
2010, **22**, 333–342

The hydrogen-bond system in pumpellyite

MARIKO NAGASHIMA[1,*], THOMAS ARMBRUSTER[1] and EUGEN LIBOWITZKY[2]

[1] Mineralogical Crystallography, Institute of Geological Sciences, University of Bern, Freiestrasse 3, 3012, Bern, Switzerland
*Corresponding author, e-mail: piemontite@gmail.com
[2] Institute of Mineralogy and Crystallography, University of Vienna – Geocenter, Althanstraße 14, 1090, Vienna, Austria

Abstract: The hydrogen-bond system of pumpellyite, simplified formula $^{W}Ca_2XY_2{}^{Z}Si_4O_{14-n}(OH)_n$ ($Z = 4$), from Oberhalbstein, Grisons, Switzerland (OHS) and Cr-rich pumpellyite from Sarany, Ural, Russia (SAR) was studied using electron-microprobe analysis (EMPA), attenuated total reflection Fourier transformed infrared spectroscopy (ATR-FTIR), and single-crystal X-ray diffraction. Structure refinements converged at R_1 factors of 2.91 % for OHS and 2.46 % for SAR. The site occupancies at *X* and *Y* are $^{X}(Mg_{0.48}Al_{0.494(3)}Fe_{0.026(3)})^{Y}(Al_{1.0})$ for OHS, and $^{X}(Mg_{0.49}Cr_{0.285(5)}Al_{0.225(5)})^{Y}(Al_{0.744(4)}Cr_{0.256(4)})$ for SAR, respectively. Both bond-valence calculations and located hydrogen sites indicated that the O5, O7, O10, and O11 positions host hydroxyl groups. One additional new hydrogen position was found in this study. Thus, two alternate hydrogen sites are linked to O5. The ATR-FTIR spectrum in the region of the OH stretching vibrations is mainly characterized by two intense OH bands at 3522 and 3379 cm^{-1} and an additional broad band around 3100 cm^{-1}. The exact number of hydroxyl groups depends on the concentration of divalent and trivalent cations at the *X* site. With only divalent cations at *X*, pumpellyite has four hydroxyl groups pfu (1) bifurcated O5–H5···O1/O5–H5···O5, (2) bifurcated O7–H7···O3/O7–H7···O7, (3) O10–H10···O5, and (4) O11–H11···O7. If there are only trivalent cations at *X*, only three OH groups pfu, (1) O5–H5′···O10, (2) bifurcated O7–H7···O3/O7–H7···O7, and (3) O11–H11···O7, are necessary for charge balance. The latter system with 3OH groups is very similar to that in sursassite.

Key-words: pumpellyite, hydrogen, macfallite, sursassite, Jahn-Teller effect, crystal structure.

1. Introduction

The crystal chemistry of many minerals formed under low-grade metamorphism and by low-temperature hydrothermal activity is not completely understood. Low-temperature silicates are often complex both structurally and compositionally. Pumpellyite is such a relatively low-temperature silicate, which has monoclinic *A*2/*m* symmetry, consists of isolated [SiO_4] tetrahedral and disilicate [$Si_2O_6(OH)$] groups, and contains two symmetrically independent chains of octahedra, oriented parallel to the *b* axis. The general formula is $^{VII}W_2{}^{VI}X^{VI}Y_2{}^{IV}Z_3O_{14-n}(OH)_n$ ($Z = 4$, Passaglia & Gottardi, 1973). The *W* site is subdivided into *W*1 and *W*2. If viewed parallel to the *b* axis (Fig. 1), the pumpellyite structure displays five-membered rings formed by corner-sharing disilicate, orthosilicate, *X*, and *Y* octahedra. Half of the rings are open and have *W*1 at their center, the others are closed and encase *W*2 (Deer *et al*., 1986). The *W* sites are predominantly occupied by Ca, and the *Z* sites by Si. Both *X* and *Y* are octahedrally coordinated but the [XO_6] octahedron is larger than the [YO_6] one. Both divalent and trivalent cations, such as Mg^{2+}, Al^{3+}, Mn^{2+}, Mn^{3+}, Fe^{2+}, Fe^{3+}, V^{3+} and Cr^{3+}, occupy *X*, whereas *Y* is occupied by trivalent cations only. In the idealized formula it is commonly assumed that one half of the *X* sites are occupied by divalent ions yielding 3.5OH and 10.5O for charge balance ($Z = 4$). However, results of analyses listed by Deer *et al*. (1986) and Passaglia & Gottardi (1973) may imply that a wide range of M^{2+}/M^{3+} ratios exist in pumpellyite-group minerals. Pumpellyite has four hydroxyl groups, if *X* is only occupied by divalent cations but it has three hydroxyl groups if only trivalent cations occupy the *X* site.

Hydrogen positions in pumpellyite-group minerals were determined for poppiite (V-analogue of pumpellyite: Brigatti *et al*., 2006) by an X-ray single-crystal study and for Cr-rich pumpellyite (Nagashima & Akasaka, 2007) by a neutron powder-diffraction study. In addition, infrared spectra of pumpellyite-(Al) were analyzed by Hatert *et al*. (2007). However, details of the hydrogen-bond system in pumpellyite have not yet been investigated.

Here, we studied the hydrogen-bond systems of pumpellyite using samples from Oberhalbstein, Grisons, Switzerland and Cr-rich pumpellyite from Sarany, Ural, Russia. The following experimental methods were used: electron microprobe analysis (EMPA), attenuated total reflection Fourier transformed infrared spectroscopy

DOI: 10.1127/0935-1221/2010/0022-2033
935-1221/10/0022-2033 $ 4.50

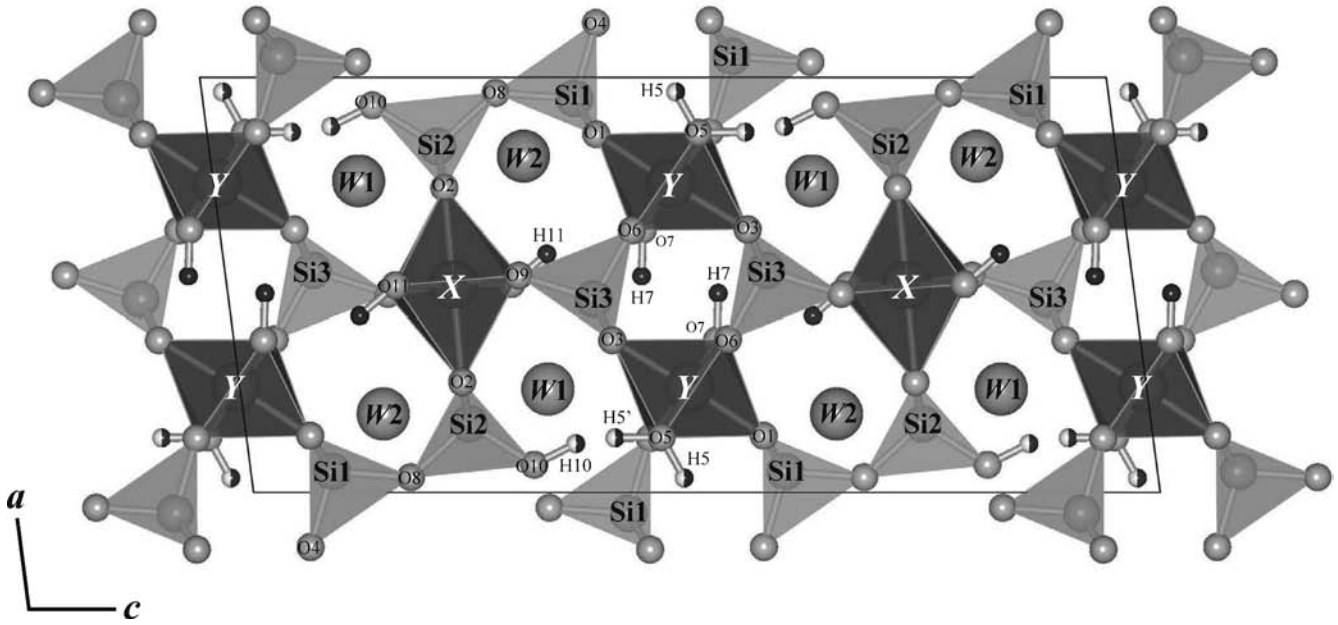

Fig 1. Crystal structure of pumpellyite (OHS) projected along [010] using the program VESTA (Momma & Izumi, 2008).

(ATR-FTIR) and single-crystal X-ray diffraction. A bond-valence analysis was also carried out. Finally, we examined the hydrogen-bond system in pumpellyite, sursassite, and macfallite.

2. Experimental methods

2.1. Samples

Pumpellyite from Alpe Flix, Val Savriez, Oberhalbstein, Grisons, Switzerland (Sample No. 484.027 supplied by the Natural History Museum of Geneva, Switzerland) and Cr-rich pumpellyite from Sarany, central Ural, Russia were studied.

Pumpellyite crystals from Oberhalbstein (OHS) occur as aggregated needles, elongated along the *b* axis, up to 1 mm in length, and are greenish white to white in color. With the polarizing microscope the crystals appear pale greenish to colorless. Cornelius (1935) performed a systematic geological and petrographical study of the area of the sample locality. However, pumpellyite was probably mistaken as zoisite in his study.

The Cr-rich pumpellyite from Sarany (SAR) was investigated by Nagashima & Akasaka (2007). The locality is *ca*. 10 km north of the Bisersk deposit (type locality of shuiskite). Ivanov *et al*. (1981) named Cr-rich pumpellyite from Bisersk shuiskite, in which all Cr^{3+} ions were assigned to the *Y* site. However, the distribution of Cr among *X* and *Y* has not been determined. Thus, it remains questionable whether shuiskite represents an independent mineral species. Cr-rich pumpellyite crystals occur as needles or prisms, elongated parallel to the *b* axis, up to 2 mm in length. With the polarizing microscope, the crystals show pleochroism from pale grayish green to pale grayish red.

2.2. Electron-microprobe analyses

The chemical composition of pumpellyite was determined using a JEOL JXA-8200 electron probe microanalyzer at the University of Bern. The abundances of Si, Ti, Al, Cr, V, Fe, Mn, Mg, Ca, Na, K, Cu, Zn, Pb and Ni were measured using an accelerating voltage of 15 kV and a beam current of 20 nA, with a beam diameter of 1 μm. The following standards were used: wollastonite (Si$K\alpha$, TAP; Ca$K\alpha$, PET), synthetic ilmenite (Ti$K\alpha$, PET), anorthite (Al$K\alpha$, TAP), synthetic eskolaite (Cr$K\alpha$, LIF), synthetic shcherbinaite (V$K\alpha$, LIF), synthetic almandine (Fe$K\alpha$, LIF), synthetic tephroite (Mn$K\alpha$, LIF), synthetic spinel (Mg$K\alpha$, TAP), albite (Na$K\alpha$, TAP), orthoclase (K$K\alpha$, PET), tennantite (Cu$K\alpha$, LIF), synthetic gahnite (Zn$K\alpha$, LIF), crocoite (Pb$L\alpha$, LIF), and synthetic bunsenite (Ni$K\alpha$, LIF). The PRZ method (modified ZAF) with $\phi(\rho Z)$ integration for the atomic number correction (Packwood & Brown, 1981; Bastin *et al*., 1984, 1986) was used for data correction. The amounts of Cu, Zn, Pb and Ni were nil.

2.3. Attenuated total reflection Fourier transform infrared spectroscopy (ATR-FTIR)

An IR powder spectrum of SAR was obtained on a BRUKER TENSOR 27 FTIR spectrometer equipped with a HARRICK MVP 2 diamond ATR accessory. A global MIR light source, a 6 mm aperture, a KBr beam splitter, and a DLaTGS detector were used to collect spectra in the wavenumber range from 370 to 4000 cm^{-1}. Sample and

background spectra were averaged from each 32 scans at 4 cm^{-1} resolution. The former were acquired from undiluted sample powder pressed to the ATR crystal, the latter from the empty ATR unit in air. Data handling was performed with OPUS 5.5 software.

2.4 Single-crystal X-ray structural analysis

The diffraction data of OHS (0.02 × 0.03 × 0.09 mm) and SAR (0.1 × 0.1 × 0.6 mm) were collected at room temperature with graphite-monochromated Mo$K\alpha$ X-radiation ($\lambda = 0.71069$ Å) using a Bruker SMART APEX II CCD diffractometer of Bruker AXS K.K.(OHS) and an Enraf-Nonius CAD4 diffractometer (SAR), respectively.

OHS: Preliminary lattice parameters and an orientation matrix were obtained from three sets of frames and refined during the integration process of the intensity data. Diffraction data were collected with ω scans with different φ settings (φ-ω scan) (Bruker, 1999). Data were processed using SAINT (Bruker, 1999). An empirical absorption correction using SADABS (Sheldrick, 1996) was applied.

SAR: Data reduction, including background and Lorentz polarization corrections, and an empirical absorption correction based on ψ scans, were done using the SDP program library (Enraf-Nonius, 1983).

For both samples structural refinements were performed using the program SHELXL-97 (Sheldrick, 2008). Scattering factors for neutral atoms were employed. At the primary stage populations of Ca at *W*1 and *W*2, Si at Si1, Si2 and Si3 for both samples and Al at *Y* for OHS were refined. However, these sites turned out to be fully occupied within one standard deviation. Thus, the site occupancies at these sites were fixed at 1.0. Mg^{2+} was assigned to *X* on the basis of the TOF neutron and X-ray Rietveld studies (Nagashima & Akasaka, 2007). Positions of the hydrogen atoms of the hydroxyl groups were derived from difference-Fourier syntheses. Subsequently, hydrogen positions were refined assuming full or half occupancy with fixed $U_{iso} = 0.05$ Å^2. In addition, a bond distance constraint of O–H = 0.980(1) Å (Franks, 1973) was applied.

3. Results

3.1. Chemical composition of pumpellyite

Table 1 shows the average chemical composition of OHS ($n = 17$). The average FeO content is 1.25 ± 0.40 wt%. There was no evidence of chemical zoning or of a domain structure with variable composition in the crystals examined. The average formula is $(Ca_{2.00}Na_{0.01})_{\Sigma 2.01}(Mg_{0.48}Al_{0.42}Fe_{0.08}Mn^{2+}_{0.01})_{\Sigma 0.99}(Al_{1.99}Ti_{0.01})_{\Sigma 2.00}Si_{3.00}O_{10.42-10.50}(OH)_{3.50-3.58}$($Z = 4$), where the total number of cations, except H ions, was normalized to 8 and the amount of OH was calculated using charge balance considerations. There are upper and lower limits to the number of O and OH, depending on whether Fe at *X* is considered Fe^{2+} or Fe^{3+}. In this study, the chemical composition of SAR was adopted from Nagashima & Akasaka (2007), *i.e.* $(Ca_{1.95}Na_{0.02}K_{0.01})_{\Sigma 1.98}(Mg_{0.49}Cr^{3+}_{0.52}Fe^{3+}_{0.01})_{\Sigma 1.02}(Al_{1.58}Cr^{3+}_{0.42})_{\Sigma 2.00}(Si_{2.95}Al_{0.05})_{\Sigma 3.00}O_{10.45}(OH)_{3.55}$($Z = 4$), where the hydrogen content was calculated based on charge balance. The oxidation state of chromium is trivalent as confirmed by optical spectroscopy (Nagashima *et al.*, in press.). The above formulae for OHS and SAR were calculated following the cation assignments suggested by Passaglia & Gottardi (1973). Accordingly, OHS and SAR should be considered pumpellyite-(Mg) and ''pumpellyite-(Cr),'' respectively. However, as it will be shown below, this arbitrary cation assignment and naming is not in agreement with the results of structure refinement.

Table 1. Composition of pumpellyite from Oberhalbstein (OHS) based on 17 point analyses.

Oxide	wt%	S.D.	Element	apfu[a]	S.D.
SiO_2	37.55	0.48	Si	3.00	0.03
TiO_2	0.08	0.04	Ti	0.01	0.00
Al_2O_3	25.55	0.49	Al	2.41	0.04
FeO[b]	1.25	0.40	Fe^{2+}	0.08	0.01
V_2O_3[b]	0.02	0.01	V^{3+}	0.00	0.00
MnO[b]	0.09	0.03	Mn^{2+}	0.01	0.00
MgO	4.02	0.22	Mg	0.48	0.03
CaO	23.37	0.23	Ca	2.00	0.01
Na_2O	0.03	0.02	Na	0.01	0.00
K_2O	0.02	0.04	K	0.00	0.00
H_2O (calc.)	6.71				
Total	98.69		Total	8.00	

[a]Total cations = 8.
[b]Total Fe as FeO, V as V_2O_3 and Mn as MnO.

Pumpellyite crystals used for EMPA and X-ray single-crystal refinements were from the same hand specimen. Therefore, average chemical compositions were used to constrain the Mg content in subsequent site population refinements.

3.2. ATR-FTIR spectrum

The ATR-FTIR spectrum between 4000 and 2500 cm^{-1} is shown in Fig. 2. Two intense bands at 3522 and 3379 cm^{-1} and an additional broad band absorption feature at *ca.* 3100 cm^{-1} have been assigned to OH stretching vibrations. Several bands are overlapping each other.

3.3. Crystal-structure solution and refinements

Crystallographic data and refinement parameters are summarized in Table 2. The refined occupancies, atomic positions and anisotropic displacement parameters are listed in Tables 3 and 4. The latter is deposited and freely available online on the GSW website of the journal (http://eurjmin.geoscienceworld.com/). Interatomic distances, angles and site distortion for the octahedral sites are presented in Table 5. In all tables, errors are shown with estimated standard deviations of 1σ (esd's). The crystal structure of pumpellyite is shown in Fig. 1.

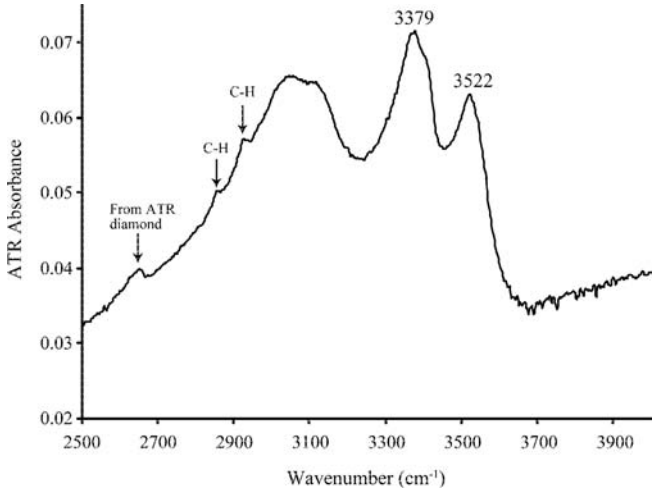

Fig 2. ATR-FTIR spectrum of Cr-rich pumpellyite (SAR) between 4000 and 1500 cm^{-1}. Weak C–H bands probably are derived from laboratory air.

Structure refinements converged at R_1 factors of 2.91 % for OHS and 2.46 % for SAR. As obtained by structure refinements, the site occupancies at X and Y are $^{X}(Mg_{0.48}Al_{0.494(3)}Fe_{0.026(3)})^{Y}(Al_{1.0})$ for OHS, and $^{X}(Mg_{0.49}Cr_{0.285(5)}Al_{0.225(5)})^{Y}(Al_{0.744(4)}Cr_{0.256(4)})$ for SAR, respectively.

Bond-valence sums were calculated using the electrostatic strength function of Brown & Altermatt (1985) and the bond-valence parameters of Brese & O'Keeffe (1991). The results are given in Table 6. Both bond valence calculations and located hydrogen sites indicated that the O5, O7, O10 and O11 positions host hydroxyl groups. The bond-valence result is consistent with previous studies (Allmann & Donnay, 1971, 1973; Yoshiasa & Matsumoto, 1985; Nagashima *et al*., 2006; Nagashima & Akasaka, 2007). Bond-valence sums for O5 and O7 are close to 1.0 v.u., suggesting full occupancy by OH, whereas bond-valence sums for O10 and O11 are about 1.3 v.u. possibly indicating partial occupancy and OH^{-}/O^{2-} disorder.

In addition to four H sites (some of them partially occupied) already reported (Brigatti *et al*., 2006; Nagashima & Akasaka, 2007), a new additional hydrogen

Table 2. Experimental details of the single-crystal X-ray diffraction analysis of pumpellyite.

Sample	OHS	SAR
Sample locality	Oberhalbstein, Grisons, Switzerland	Sarany, Ural, Russia
Crystal size (mm)	0.02 × 0.03 × 0.09	0.1 × 0.1 × 0.6
Space group	*A*2/*m*	*A*2/*m*
Cell parameters		
a (Å)	8.8177 (2)	8.805 (2)
b (Å)	5.8999 (1)	5.931 (2)
c (Å)	19.1056 (4)	19.133 (5)
β (°)	97.401 (1)	97.49 (4)
V (Å^3)	985.66 (1)	990.7 (5)
D_{calc} (g/cm^3)	3.17	3.29
Radiation	Mo$K\alpha$ ($\lambda = 0.71069$ Å)	Mo$K\alpha$ ($\lambda = 0.71069$ Å)
Monochromator	Graphite	Graphite
Diffractometer	Bruker APEX CCD	Enraf-Nonius CAD4
Scan type	$\varphi-\omega$ scan (Bruker, 1999)	ω scan (Enraf-Nonius, 1983)
Absorption correction	SADABS (Sheldrick, 1996)	ψ-scan (Enraf-Nonius, 1983)
θ_{min} (°)	2.2	2.2
θ_{max} (°)	32.9	29.9
μ (mm^{-1})	2.63	2.43
Collected reflections	14,185	2136
Unique reflections	1958	1566
R_{int} (%)	4.54	3.12
R_σ (%)	3.55	3.06
Miller index limits	$-13 \le h \le 13$, $-8 \le k \le 8$, $-28 \le l \le 27$	$-1 \le h \le 12$, $-8 \le k \le 1$, $-26 \le l \le 26$
Refinement on F^2 using	SHELXL-97 (Sheldrick, 2008)	SHELXL-97 (Sheldrick, 2008)
R_1 (%)	2.91	2.46
wR_2 (%)	7.40	6.89
No. of parameters	133	134
Weighting scheme[a]	$w = 1/[\sigma^2(F_o^2) + (0.0319P)^2 + 1.56P]$	$w = 1/[\sigma^2(F_o^2) + (0.0381P)^2 + 0.83P]$
$\Delta\rho_{max}$ (e Å^{-3})	0.728 at 0.86 Å from O8	0.750 at 0.75 Å from *W*1
$\Delta\rho_{min}$ (e Å^{-3})	−0.644 at 0.57 Å from Si3	−0.468 at 0.83 Å from *Y*

Chemical formulae of OHS and SAR are represented as $(Ca_{2.00}Na_{0.01})_{\Sigma 2.01}(Mg_{0.48}Al_{0.42}Fe_{0.08}Mn^{2+}_{0.01})_{\Sigma 0.99}(Al_{1.99}Ti_{0.01})_{\Sigma 2.00}Si_{3.00}O_{10.42-10.50}(OH)_{3.50-3.58}$ ($Z = 4$) and $(Ca_{1.95}Na_{0.02}K_{0.01})_{\Sigma 1.98}(Mg_{0.49}Cr^{3+}_{0.52}Fe^{3+}_{0.01})_{\Sigma 1.02}(Al_{1.58}Cr^{3+}_{0.42})_{\Sigma 2.00}(Si_{2.95}Al_{0.05})_{\Sigma 3.00}O_{10.45}(OH)_{3.55}$ ($Z = 4$, Nagashima & Akasaka, 2007), respectively.

[a]The function of the weighting scheme is $w = 1/(\sigma^2(F_0^2) + (a \cdot P)^2 + b \cdot P)$, where ($P = (\mathrm{Max}(F_o^2) + 2F_c^2)/3$, and the parameters a and b are chosen to minimize the differences in the variances for reflections in different ranges of intensity and diffraction angle.

Table 3. Site occupancies, atomic positions and equivalent displacement parameters (Å^2).

Site		OHS	SAR	Site		OHS	SAR
*W*1	*x*	0.24963 (6)	0.25044 (7)	O6	*x*	0.3693 (2)	0.3701 (2)
	y	1/2	1/2		*y*	1/2	1/2
	z	0.33951 (3)	0.33951 (3)		*z*	0.04524 (10)	0.04488 (10)
	U_{eq}	0.01245 (12)	0.00970 (14)		U_{eq}	0.0109 (4)	0.0089 (4)
Occup.		$Ca_{1.0}$	$Ca_{1.0}$	O7	*x*	0.3671 (2)	0.3696 (2)
*W*2	*x*	0.18990 (7)	0.18851 (8)		*y*	0	0
	y	1/2	1/2		*z*	0.03295 (10)	0.03352 (11)
	z	0.15427 (3)	0.15438 (3)		U_{eq}	0.0130 (4)	0.0113 (4)
	U_{eq}	0.01573 (13)	0.01278 (14)	O8	*x*	0.0369 (2)	0.0361 (2)
Occup.		$Ca_{1.0}$	$Ca_{1.0}$		*y*	0	0
X	*x*	1/2	1/2		*z*	0.17578 (10)	0.17598 (10)
	y	1/4	1/4		U_{eq}	0.0125 (4)	0.0103 (4)
	z	1/4	1/4	O9	*x*	0.4779 (2)	0.4776 (2)
	U_{eq}	0.0095 (2)	0.0067 (2)		*y*	1/2	1/2
Occup.		$Mg_{0.48}Al_{0.494(3)}Fe_{0.026(3)}$	$Mg_{0.49}Cr_{0.285(5)}Al_{0.225(5)}$		*z*	0.17645 (10)	0.17645 (11)
Y	*x*	0.25510 (6)	0.25439 (5)		U_{eq}	0.0146 (4)	0.0106 (4)
	y	0.24583 (9)	0.24651 (8)	O10	*x*	0.0672 (2)	0.0670 (3)
	z	0.49578 (3)	0.49560 (2)		*y*	0	0
	U_{eq}	0.00814 (12)	0.00579 (15)		*z*	0.31357 (11)	0.31357 (11)
Occup.		$Al_{1.0}$	$Al_{0.744\ (4)}Cr_{0.256\ (4)}$		U_{eq}	0.0180 (4)	0.0142 (5)
Si1	*x*	0.05043 (8)	0.05104 (9)	O11	*x*	0.5014 (2)	0.5025 (2)
	y	0	0		*y*	1/2	1/2
	z	0.08955 (4)	0.09034 (4)		*z*	0.31405 (10)	0.31484 (11)
	U_{eq}	0.00896 (14)	0.00635 (16)		U_{eq}	0.0133 (4)	0.0104 (4)
Occup.		$Si_{1.0}$	$Si_{1.0}$	H5	*x*	0.035 (4)	0.021 (3)
Si2	*x*	0.16614 (8)	0.16596 (9)		*y*	0	0
	y	0	0		*z*	0.477 (4)	0.464 (5)
	z	0.24753 (4)	0.24784 (4)		U_{iso}	0.05	0.05
	U_{eq}	0.00996 (15)	0.00724 (16)	Occup.		$H_{0.5}$ (half)	$H_{0.5}$ (half)
Occup.		$Si_{1.0}$	$Si_{1.0}$	H5′	*x*	0.132 (11)	0.163 (11)
Si3	*x*	0.46571 (8)	0.46522 (9)		*y*	0	0
	y	0	0		*z*	0.4065 (6)	0.411 (2)
	z	0.40292 (4)	0.40279 (4)		U_{iso}	0.05	0.05
	U_{eq}	0.00912 (15)	0.00637 (16)	Occup.		$H_{0.5}$ (half)	$H_{0.5}$ (half)
Occup.		$Si_{1.0}$	$Si_{1.0}$	H7	*x*	0.4791 (3)	0.4815 (5)
O1	*x*	0.13735 (15)	0.13779 (16)		*y*	0	0
	y	0.2254 (2)	0.2243 (3)		*z*	0.041 (2)	0.044 (3)
	z	0.07079 (7)	0.07186 (7)		U_{iso}	0.05	0.05
	U_{eq}	0.0119 (3)	0.0091 (3)	Occup.		$H_{1.0}$ (full)	$H_{1.0}$ (full)
O2	*x*	0.26649 (15)	0.26624 (17)	H10	*x*	0.118 (9)	0.103 (12)
	y	0.2313 (2)	0.2306 (3)		*y*	0	0
	z	0.24593 (7)	0.24605 (7)		*z*	0.3623 (16)	0.3642 (12)
	U_{eq}	0.0132 (3)	0.0098 (3)		U_{iso}	0.05	0.05
O3	*x*	0.36708 (15)	0.36684 (17)	Occup.		$H_{0.5}$ (half)	$H_{0.5}$ (half)
	y	0.2228 (2)	0.2228 (3)	H11	*x*	0.574 (4)	0.562 (5)
	z	0.41739 (7)	0.41651 (8)		*y*	1/2	1/2
	U_{eq}	0.0119 (3)	0.0097 (3)		*z*	0.3575 (13)	0.3618 (12)
O4	*x*	0.1311 (2)	0.1307 (2)		U_{iso}	0.05	0.05
	y	1/2	1/2	Occup.		$H_{1.0}$ (full)	$H_{1.0}$ (full)
	z	0.44488 (10)	0.44461 (10)				
	U_{eq}	0.0099 (3)	0.0077 (4)				
O5	*x*	0.1332 (2)	0.1303 (2)				
	y	0	0				
	z	0.45788 (10)	0.45777 (11)				
	U_{eq}	0.0116 (4)	0.0094 (4)				

Note: All oxygen occupancies were fixed at 1.0.

position, H5′, has been found in both studied samples (OHS and SAR). Thus, O5 may form hydroxyl groups with two different O–H orientations.

4. Discussion

4.1. Nomenclature of pumpellyite-group minerals

''The unit-cell content should be calculated on the basis of 56 oxygens'' was proposed by Passaglia & Gottardi (1973) as the first step for the calculation of pumpellyite chemical-formula. This rule can only be applied if the amount of H_2O and the oxidation state of the transition elements, such as Fe and Mn, has been directly determined. If the chemical compositions is evaluated using conventional microprobe analysis, the pumpellyite formula must be normalized to a total of 32 cations ($Z = 1$) instead of O = 56 because of the uncertain oxidation state of transition elements and unknown water content. According to the nomenclature of pumpellyite-group minerals (Passaglia & Gottardi, 1973), the root name is determined by the dominant cation at *Y*, and the dominant cation at *X* is represented as a suffix designation. The rule to assign the cations to the *X* and *Y* octahedral sites proposed by Passaglia & Gottardi (1973) is: (a) Al and Ti are assigned to *Y*; if this assignment is not enough for full occupancy of *Y*, Fe^{3+} is added until the site is filled. (b) Mn, Fe^{2+} and Mg are assigned to *X* together with possibly remaining Fe^{3+} and Al. Based on this precept, the amount of Al at *Y* is in many cases overestimated. Following this procedure the chemical formulae of OHS and SAR lead to the names pumpellyite-(Mg) and ''pumpellyite-(Cr),'' respectively. ''Pumpellyite-(Cr)'' has not yet been reported as an independent species. However, based on site occupancies obtained by X-ray structure-refinements, OHS and SAR must be named pumpellyite-(Al) and pumpellyite-(Mg), respectively. Thus, the names determined from the chemical formula (Passaglia & Gottardi, 1973), and the refined site-occupancies, are inconsistent. The discrepancy is caused by the Al distribution over *X* and *Y*. Refined site-occupancies clearly indicate that Al occupies *X* before *Y* is filled with Al (*e.g.*, Artioli & Geiger, 1994; Artioli *et al.*, 1996; Brigatti *et al.*, 2006; Nagashima *et al.*, 2006; Nagashima & Akasaka, 2007). We have to consider that, not only for pumpellyite, mineral naming is a compromise between a rather arbitrary rule of building up a chemical formula from analytical results only and a more realistic formula obtained by a combination of chemical analyses and cation distribution by structure refinement. Probably the best way out of this dilemma is to state only the mineral group (*e.g.*, pumpellyite) whenever analytical data are not sufficient for assignment of a mineral species.

4.2. Cation distribution among the octahedral sites

Previous studies suggested that the mean *Y*–O distance and the mean ionic radius of atoms at the *Y* site are positively correlated whereas the mean *X*–O distance and the mean ionic radius of ions at the *X* site show no correlation (Nagashima *et al.*, 2006; Nagashima & Akasaka, 2007). The regression line of the <*Y*-O> distance *versus* the mean ionic radius at *Y* is $y = 0.927x + 1.426$, where *y* is <*Y*-O> distance (Å) and *x* represents the mean ionic radius (Å) (Nagashima & Akasaka, 2007). According to this function, the expected *Y*-O distances are 1.92 Å for OHS and 1.94 Å for SAR. They agree well with the observed values (1.922 Å for OHS and 1.936 Å for SAR) in this study.

The polyhedral distortions at *X* and *Y* were examined by bond-length distortion parameters $<\lambda_{oct}>$ defined by Robinson *et al.* (1971), *DI*(oct) by Baur (1974), and the angular distortion parameter $\sigma_\theta(\text{oct})^2$ of Robinson *et al.* (1971). All distortion parameters for the *Y* site of OHS are larger than those of SAR (Table 5). These results confirm that expansion of the *Y* octahedra, due to substitution of larger cations for Al, makes the *Y* octahedron geometrically more regular (Nagashima *et al.*, 2006; Nagashima & Akasaka, 2007).

4.3. Hydrogen positions and hydrogen bonds

The positions of hydrogen atoms and hydrogen bonds in pumpellyite are shown in Fig. 3. In general, there are four hydroxyl groups (Fig. 3a). All donor oxygen-hydrogen bonds of pumpellyite are located on mirror planes parallel to (010) as suggested by Yoshiasa & Matsumoto (1985). The relationship between donor and acceptor oxygens and their hydrogen bonds can be summarized as follows: (1) bifurcated O5–H5···O1/O5–H5···O5, (2) O5–H5′···O10, (3) bifurcated O7–H7···O3/O7–H7···O7, (4) O10–H10···O5, and (5) O11–H11···O7. The H5 and H5′ sites are assumed to be half-occupied (Fig. 3).

Bond valences of O5 and O7 are lower than those of O10 and O11 (Table 6). Therefore, O5 and O7 are privileged to act simultaneously as donor and as acceptor. Ferraris & Ivaldi (1988) have shown that for short O–H···O donor acceptor distances, the acceptor benefits from additional *ca.* 0.25 v.u. O5 acts as donor for H5 or H5′ and forms the hydrogen bond system O5–H5···O5 or O5–H5′···O10. O7 acts as donor for H7, and forms the O7–H7···O7 hydrogen bond, crossing the narrow channels. This hydrogen bond may be bifurcated connecting H7 to both O7 and O3. In addition, O5 and O7 act as acceptors of H10 and H11, respectively.

The IR spectrum of SAR in the region of the OH stretching vibration is mainly characterized by two bands at 3522 and 3379 cm^{-1}, and one broad band at *ca.* 3100 cm^{-1} (Fig. 2). The associated OH···O distances were estimated using the correlation between observed OH stretching wavenumber and the O···O separation given by Libowitzky (1999). The estimated O···O separations are 2.93 (3522 cm^{-1}), 2.78 (3379 cm^{-1}) and 2.67 Å (3100 cm^{-1}). Yoshiasa & Matsumoto (1985) suggested the following substitutional mechanism: $M^{3+} + O^{2-} \leftrightarrow M^{2+} + OH^-$. Thus, depending on M^{2+} at *X*, pumpellyite is assumed to have two different hydroxyl systems. H5′ is an indicator of an additional new hydrogen-bond system. These two systems might also be the reason for the complex IR spectra.

Table 5. Selected interatomic distances (Å), angles (°), volume and distortion.

		OHS	SAR			OHS	SAR
W1–O2	×2	2.409 (1)	2.416 (2)	Si1–O1	×2	1.599 (1)	1.597 (2)
–O3	×2	2.359 (1)	2.352 (2)	–O4		1.650 (2)	1.652 (2)
–O4		2.385 (2)	2.389 (2)	–O8		1.667 (2)	1.661 (2)
–O8		2.506 (2)	2.502 (2)		Mean	1.629	1.627
–O11		2.333 (2)	2.328 (2)				
	Mean	2.394	2.394	Si2–O2	×2	1.629 (1)	1.631 (2)
				–O8		1.666 (2)	1.670 (2)
W2–O1	×2	2.279 (1)	2.276 (2)	–O10		1.624 (2)	1.621 (2)
–O2	×2	2.394 (1)	2.405 (2)		Mean	1.637	1.638
–O6		2.773 (2)	2.796 (2)				
–O9		2.520 (2)	2.525 (2)	Si3 –O3	×2	1.619 (1)	1.620 (2)
–O10		2.424 (2)	2.408 (2)	–O6		1.651 (2)	1.652 (2)
	Mean	2.438	2.442	–O9		1.655 (2)	1.659 (2)
					Mean	1.636	1.638
X–O2	×2	2.053 (1)	2.053 (2)	*Y*–O1		1.883 (1)	1.898 (2)
–O9	×2	2.029 (1)	2.036 (2)	–O3		1.902 (1)	1.918 (2)
–O11	×2	1.916 (1)	1.932 (1)	–O4		2.029 (1)	2.030 (2)
	Mean	1.999	2.007	–O5		1.893 (1)	1.910 (2)
$V^{(VI)}$ (Å^3)		10.58	10.68	–O6		1.940 (1)	1.953 (2)
DI (oct)		0.028	0.025	–O7		1.884 (1)	1.904 (2)
$<\lambda$ oct$>$		1.007	1.007		Mean	1.922	1.936
σ_θ (oct)^2		18.98	18.34	$V^{(VI)}$ (Å^3)		9.31	9.52
				DI (oct)		0.022	0.019
O5···O1		–	2.867 (2)	$<\lambda$ oct$>$		1.012	1.011
O5···O5		3.014 (2)	2.974 (3)	σ_θ (oct)^2		37.34	35.64
O7···O3		2.915 (2)	2.902 (2)				
O7···O7		2.800 (2)	2.772 (2)	O1–Si1–O1		112.6 (1)	112.9 (1)
O10···O5		2.744 (3)	2.734 (3)	O1–Si1–O4	×2	112.27 (6)	112.12 (7)
O11···O7		3.003 (3)	2.972 (3)	O1–Si1–O8	×2	108.61 (6)	108.68 (7)
H5–H5		1.14 (8)	1.47 (12)	O4–Si1–O8		101.8 (1)	101.7 (1)
H7–H7		1.66 (5)	1.76 (7)				
				O2–Si2–O2		113.8 (1)	114.0 (1)
O5–H5–O1		–	124 (1)	O2–Si2–O8	×2	107.48 (6)	107.29 (7)
O5–H5–O5		165 (1)	143 (1)	O2–Si2–O10	×2	111.23 (6)	111.33 (7)
O5–H5′–O10		162 (2)	137 (2)	O8–Si2–O10		105.1 (1)	105.0 (1)
O7–H7–O3		128.1 (9)	129 (1)				
O7–H7–O7		128.7 (9)	124 (1)	O3–Si3–O3		108.5 (1)	109.3 (1)
O10–H10–O5		157 (2)	169 (2)	O3–Si3–O6	×2	110.41 (7)	110.34 (7)
O11–H11–O7		153.9 (9)	165 (1)	O3–Si3–O9	×2	112.81 (6)	112.37 (7)
				O6–Si3–O9		101.8 (1)	101.9 (1)

Note: $DI(\text{oct}) = 1/6\Sigma|R_i - R_{\text{av.}}|/R_{\text{av.}}$ (R_i: each bond length, $R_{\text{av.}}$: average distance for an octahedron) (Baur, 1974), $\lambda_{\text{oct}} = \sum_{i=1}^{6} (l_i - l_0)^2 \Big/ 6$ (l_i: each bond length, l_0: center-to-vertex distance for an octahedron with O_h symmetry, whose volume is equal to that of a distorted octahedron with bond lengths l_i) (Robinson *et al*., 1971), and $\sigma_\theta(\text{oct})^2 = \sum_{i=1}^{12} (\theta_i - 90°)^2 \Big/ 11$ (θ_i: O–*M*–O angle) (Robinson *et al*., 1971).

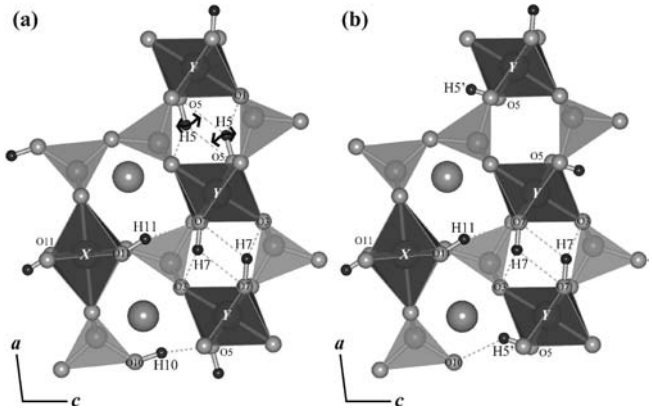

Fig 3. Hydrogen-bond system with 4OH (a) and 3OH (b), in pumpellyite (SAR) projected along [010]. Dashed lines indicate H···O bonds.

A similar IR spectrum as described here has also been reported for pumpellyite-(Al) by Hatert *et al*. (2007). According to their description, the estimated OH···O distances using the correlation by Libowitzky (1999) are in good agreement with those determined from the X-ray Rietveld refinement. Hatert *et al*. (2007) suggested that the observed wavenumbers correspond to the following O-H···O distances: 2.65 (3010 cm^{-1}), 2.68 (3127 cm^{-1}), 2.80 (3407 cm^{-1}), 2.89 (3499 cm^{-1}), and 2.98 Å (3542 cm^{-1}). As result of their structural refinement, the distances between oxygen atoms involved in hydrogen bonds are as follows: 2.708 (O7···O7), 2.771 (O10···O5), 2.867 (O5···O5), and 2.915 Å (O11···O7) (Hartert *et al*., 2007). As shown in this study, two different systems of hydrogen bonds may develop in pumpellyite. Thus, the corresponding relations between IR

Table 6. Calculated bond valences (v.u.).

OHS									
Anion \ Cation	*W1*	*W2*	*X*	*Y*	Si1	Si2	Si3	$\Sigma_C v$	Anion chemistry
O1		0.393[a]		0.533	1.117[a]			2.043	O^{2-}
O2	0.286[a]	0.297[a]	0.357[a]			1.030[a]		1.970	O^{2-}
O3	0.323[a]			0.507			1.058[a]	1.888	O^{2-}
O4	0.303			0.363[b]	0.973			2.002	O^{2-}
O5				0.519[b]				1.038	OH^-
O6		0.118		0.459[b]			0.971	2.007	O^{2-}
O7				0.532[b]				1.064	OH^-
O8	0.226				0.930	0.932		2.088	O^{2-}
O9		0.218	0.380[a,b]				0.960	1.938	O^{2-}
O10		0.276				1.044		1.320	OH^-
O11	0.344		0.504[a,b]					1.352	OH^-
$\Sigma_A v$	2.091	1.992	2.482	2.913	4.137	4.036	4.047		
SAR									
O1		0.396[a]		0.539	1.123[a]			2.058	O^{2-}
O2	0.281[a]	0.289[a]	0.374[a]			1.025[a]		1.969	O^{2-}
O3	0.329[a]			0.511			1.056[a]	1.896	O^{2-}
O4	0.300			0.380[b]	0.968			2.028	O^{2-}
O5				0.522[b]				1.044	OH^-
O6		0.111		0.466[b]			0.968	2.011	O^{2-}
O7				0.530[b]				1.060	OH^-
O8	0.228				0.945	0.922		2.095	O^{2-}
O9		0.216	0.390[a,b]				0.950	1.946	O^{2-}
O10		0.287				1.053		1.340	OH^-
O11	0.349		0.507[a,b]					1.363	OH^-
$\Sigma_A v$	2.097	1.984	2.542	2.948	4.159	4.025	4.030		

Note: $\Sigma_A v$ is the valence of bonds emanating from a cation summed over the bonded anions. $\Sigma_C v$ is the valence of bonds reaching an anion.
[a]Two bonds per cation.
[b]Two bonds per anion.

bands and bond distances might be more complex than suggested by Hatert *et al*. (2007).

The hydrogen-bond models can be separated into a 3OH and a 4OH pfu system in order to maintain charge-balance based on the M^{2+} substitution mechanism (Yoshiasa & Matsumoto, 1985). The 4OH system has the following arrangement: (1) bifurcated O5–H5···O1/O5–H5···O5, (2) bifurcated O7–H7···O3/O7–H7···O7, (3) O10–H10···O5 and (4) O11–H11···O7 as suggested by Yoshiasa & Matsumoto (1985) (Fig. 3a). On the other hand, the 3OH system has (1) O5–H5′···O10, (2) bifurcated O7–H7···O3/O7–H7···O7, and (3) O11–H11···O7 (Fig. 3b). In the latter case, O10 acts only as acceptor. If both systems occur side by side H5, H5′ and H10 are assumed to be half occupied. Two of the OH groups (at O5 and O7) are located in the narrow channels between edge-connected chains of [YO_6] octahedra. H5–H5 distances between two adjacent OH groups are very short (1.1–1.5 Å, Table 5) and are similar to corresponding distances (*ca*. 1.33 Å) in lawsonite. For *Cmcm* lawsonite at RT (Libowitzky & Armbruster, 1995), the short H–H distances in a topologically similar structural environment were explained by dynamic proton disorder (Libowitzky & Rossman, 1996). The *Pmcn* lawsonite low-temperature phase with ordered OH orientations yielded at 155 K a corresponding H–H separation of 1.85 Å. Thus, in contrast to lawsonite where dynamic disorder was required by proton-proton repulsion and full occupancy, this is not necessarily required in pumpellyite. In addition, O5–H5′ is active whenever H10 is vacant. The hydroxyl group at O10 terminates the disilicate unit and, therefore, O10–H10 represents a so-called silanol group. Nyfeler & Armbruster (1998) predicted silanol groups with lengthened Si–O bonds. However, Si2–O10 distances in OHS and SAR are the shortest ones within the Si2 tetrahedron (Table 5). These short distances are explained by disorder due to the half occupied H10 site.

The similarity of the hydrogen-bond system of pumpellyite, sursassite and macfallite was pointed out by Nagashima *et al*., 2008, 2009). Macfallite ($Z = 2$, space group $P2_1/m$, $Ca_2Mn^{3+}{}_3Si_3O_{11}(OH)_3$) and sursassite ($Z = 2$, space group $P2_1/m$, $Mn^{2+}{}_2Al_3Si_3O_{11}(OH)_3$) are iso-structural and generally have three OH groups pfu. Their structures may be derived from that of pumpellyite by a $1/2(a + c)$ shift (Mellini *et al*., 1984; Moore *et al*., 1985; Ferraris *et al*., 1986). The structural similarity of pumpellyite, macfallite and sursassite was elaborated by Moore *et al*. (1985) and Ferraris *et al*. (1986). Subordinate divalent cations are at *M*1

in sursassite (Nagashima *et al*., 2009) and macfallite (Nagashima *et al*., 2008) and at *X* in pumpellyite. [XO_6]-octahedra in pumpellyite and [$M1O_6$]-octahedra in sursassite and macfallite are topologically similar to each other, and [YO_6]-octahedra in pumpellyite are topologically similar to [$M2O_6$]- and [$M3O_6$]-octahedra in sursassite and macfallite. The hydrogen-bond systems in macfallite and sursassite were resolved by Nagashima *et al*., 2008, 2009). In the case of macfallite, there is only one OH group in the narrow channels between edge-connected chains of [$M2O_6$] and [$M3O_6$] octahedra, although in the case of pumpellyite and sursassite, there are two hydroxyl groups located in the channel.

The IR spectra of macfallite and sursassite showed a broad band around 2900 cm^{-1} (Fig. 2 in Nagashima *et al*., 2008) and 2950 cm^{-1} (Fig. 1 in Nagashima *et al*., 2009), which are similar to the one of pumpellyite (*ca*. 3100 cm^{-1}). In macfallite the broad band was assigned to the hydrogen bond O6···O11 with a distance of about 2.63 Å, crossing the narrow channel. In contrast, the broad IR band at 2950 cm^{-1} in sursassite was assigned to O6···O10 with a distance of 2.66–2.67 Å, which represents the open edge of the Mn1 channel. In the case of pumpellyite (this study), this broad band is assigned to O10···O5, which is the open edge of the *W*1 channel. This edge is topologically very similar to O6···O10 in sursassite. The O5···O5 and O7···O7 distances of pumpellyite, crossing the narrow channel, are considerably longer. The possible reason for the different assignment of the broad IR band (2900 cm^{-1}) in macfallite are distortions due to the Jahn-Teller effect of Mn^{3+} at the *M*2 and *M*3 sites. The *M*2 and *M*3 sites in sursassite are mainly occupied by Al, as is the *Y* site of OHS and SAR pumpellyite. However, in the case of pumpellyite, Al at *Y* may also be substituted by Mn^{3+}. It is known that in pumpellyite the size and electronic structure of the ion (Cr^{3+}, Fe^{3+}, Mn^{3+}, and Al) at *Y* are crucial factors determining the size of the channels because the volume of the [YO_6] octahedron simply reflects the substitution at *Y*. This implies that Mn^{3+} substituting for Al at *Y* in Mn^{3+}-rich pumpellyite, *i.e*. okhotskite, leads to an increased volume of the [YO_6] octahedra simultaneously shortening the distance across the narrow channels. Thus, depending on chemistry the assignment of OH-specific IR bands in pumpellyite may be different.

The 3OH systems of isostructural macfallite $Ca_2Mn^{3+}{}_3Si_3O_{11}(OH)_3$ (Fig. 4 in Nagashima *et al*., 2008) and sursassite $Mn^{2+}{}_2Al_3Si_3O_{11}(OH)_3$ (Fig. 6 in Nagashima *et al*., 2009) are different. The influence of Mn^{3+} Jahn-Teller distortion on hydrogen bonds has been described above. Isostructural mozartite $CaMn^{3+}SiO_4(OH)$ and vuagnatite $CaAlSiO_4(OH)$ also show a different arrangement of hydrogen-bond acceptors and donors because of the active role of the Mn^{3+} Jahn-Teller effect (Nyfeler *et al*., 1997). Thus, the investigation of the hydrogen-bond system in Mn^{3+}-rich pumpellyite-group minerals and the systematic understanding of the hydrogen-bond systems in pumpellyite, sursassite, macfallite and other structurally and compositionally related minerals are mandatory.

Acknowledgements: We thank Dr. E. Gnos at the Natural History Museum of Geneva, Switzerland, for supplying us with the pumpellyite (Sample No. 484.027). We also thank chief editor Prof. Oberhänsli, associate editor Prof. M. Pasero, and an anonymous reviewer for their constructive comments on this manuscript. This research was supported by the Japan Society for the Promotion of Science (JSPS) for research abroad to M. Nagashima.

References

Allmann, R. & Donnay, G. (1971): Structural relations between pumpellyite and ardennite. *Acta Crystallogr. B*, **27**, 1871–1875.

—, — (1973): The crystal structure of julgoldite. *Mineral. Mag.*, **39**, 371–281.

Artioli, G. & Geiger, C.A. (1994): The crystal chemistry of pumpellyite: an X-ray Rietveld refinement and ^{57}Fe Mössbauer study. *Phys. Chem. Minerals*, **20**, 443–453.

Artioli, G., Pavese, A., Belotto, M., Collins, S.P., Luchetti, G. (1996): Mn crystal chemistry in pumpellyite: a resonant-scattering powder diffraction Rietveld study using synchrotron radiation. *Am. Mineral.*, **81**, 603–610.

Bastin, G.F., van Loo, F.J.J., Heijlingers, H.J.M. (1984): Evaluation of the use of Gaussian $\phi(\rho z)$ curves in quantitative electron probe microanalysis: a new optimization. *X-ray Spectrom.*, **13**, 91–97.

Bastin, G.F., Heijlingers, H.J.M., van Loo, F.J.J. (1986): A further improvement in the Gaussian $\phi(\rho z)$ approach for matrix correction in quantitative electron probe microanalysis. *Scanning*, **8**, 45–67.

Baur, H. (1974): The geometry of polyhedral distortions. Predictive relationships for the phosphate group. *Acta Crystallogr. B*, **30**, 1195–1215.

Brese, N.E. & O'Keeffe, M. (1991): Bond-valence parameters for solids. *Acta Crystallogr. B*, **47**, 192–197.

Brigatti, M.F., Caprilli, E., Marchesini, M. (2006): Poppiite, the V^{3+} end-member of the pumpellyite group: description and crystal structure. *Am. Mineral.*, **91**, 584–588.

Brown, I.D. & Altermatt, D. (1985): Bond-valence parameters obtained from a systematic analysis of the inorganic crystal structure database. *Acta Crystallogr. B*, **41**, 244–247.

Bruker (1999): SMART and SAINT-Plus. Versions 6.01. Bruker AXS Inc., Madison, WI, USA.

Cornelius, H.P. (1935): Geologie der Err-Julier-Gruppe I. Teil: Das Baumaterial (Stratigraphie und Petrographie, excl. Quartär). Beiträge zur Geologischen Karte der Schweiz. Neue Folge, 70. I. Teil., Geologische Kommission der Schweizerischen Naturforschenden Gesellschaft, 321 p.

Deer, W.A., Howie, R.A., Zussman, J. (1986): Rock-forming minerals. 1B (2^{nd} ed.), disilicates and ring silicates. Geological Society Publishing House, UK, 629 p.

Enraf-Nonius (1983): Structure determination package (SDP) (computer program). Enraf Nonius, Delft, The Netherlands.

Ferraris, G. & Ivaldi, G. (1988): Bond valence vs bond length in O. . .O hydrogen bonds. *Acta Crystallogr. B*, **44**, 341–344.

Ferraris, G., Mellini, M., Merlino, S. (1986): Polysomatism and the classification of minerals. *Rend. Soc. Ital. Mineral. Petrol.*, **44**, 181–192.

Franks, F. (1973): Water: a comprehensive treatise, Vol. 2. Plenum, New York, 684 p.

Hatert, F., Pasero, M., Perchiazzi, N., Theye, T. (2007): Pumpellyite-(Al), a new mineral from Bertrix, Belgian Ardennes. *Eur. J. Mineral.*, **19**, 247–253.

Ivanov, O.K., Arkhangel'skaya, V.A., Miroshnikova, L.O., Shilova, T.A. (1981): Shuiskite, the chromium analogue of pumpellyite, from the Bisersk deposit, Urals. *Zap. Vses. Mineral. Obshchest*, **110**, 508–512 (in Russian).

Libowitzky, E. (1999): Correlation of O–H stretching frequencies and O–H···O hydrogen bond lengths in minerals. *Mh. Chem.*, **130**, 1047–1059.

Libowitzky, E. & Armbruster, T. (1995): Low-temperature phase transitions and the role of hydrogen bonds in lawsonite. *Am. Mineral.*, **80**, 1277–1285.

Libowitzky, E. & Rossman, G.R. (1996): FTIR spectroscopy of lawsonite between 82 and 325 K. *Am. Mineral.*, **81**, 1080–1091.

Mellini, M., Merlino, S., Pasero, M. (1984): X-ray and HRTEM study of sursassite: crystal structure, stacking disorder and sursassite-pumpellyite intergrowth. *Phys. Chem. Minerals*, **10**, 99–105.

Momma, K. & Izumi, F. (2008): VESTA: a three-dimensional visualization system for electronic and structural analysis. *J. Appl. Crystallogr.*, **41**, 653–658.

Moore, P.B., Shen, J., Araki, T. (1985): Crystal chemistry of the $^{2}_{\infty}\left[M_2^{3+}\phi_2(TO_4)_2\right]$ sheet: structural principles and crystal structures of ruizite, macfallite and orientite. *Am. Mineral.*, **70**, 171–181.

Nagashima, M. & Akasaka, M. (2007): The distribution of chromium in chromian pumpellyite from Sarany, Urals, Russia: a TOF neutron and X-ray Rietveld study. *Can. Mineral.*, **45**, 837–846.

Nagashima, M., Ishida, T., Akasaka, M. (2006): Distribution of Fe among octahedral sites and its effect on the crystal structure of pumpellyite. *Phys. Chem. Minerals*, **33**, 178–191.

Nagashima, M., Rahmoun, N.-S., Alekseev, E.V., Geiger, C.A., Armbruster, T., Akasaka, M. (2008): Crystal chemistry of macfallite: relationships to sursassite and pumpellyite. *Am. Mineral.*, **93**, 1851–1857.

Nagashima, M., Akasaka, M., Minakawa, T., Libowitzky, E., Armbruster, T. (2009): Sursassite: hydrogen bonding, cation order, and pumpellyite intergrowth. *Am. Mineral.*, **94**, 1440–1449.

Nagashima, M., Akasaka, M., Ikeda, K., Kyono, A., Makino, K. (in press): X-ray single-crystal and optical study of chromian pumpellyite from Sarany, Urals, Russia. *J. Mineral. Petrol. Sci.*

Nyfeler, D. & Armbruster, T. (1998): Silanol groups in minerals and inorganic compounds. *Am. Mineral.*, **83**, 119–125.

Nyfeler, D., Hoffmann, C., Armbruster, T., Kunz, M., Libowitzky, E. (1997): Orthorhombic Jahn-Teller distortion and Si–OH in mozartite, $CaMn^{3+}O[SiO_3OH]$: a single-crystal X-ray, FTIR, and structure modelling study. *Am. Mineral.*, **82**, 841–848.

Packwood, R.H. & Brown, J.D. (1981): A Gaussian expression to describe $\phi(\rho z)$ curves for quantitative electron probe microanalysis. *X-ray Spectrom.*, **10**, 138–146.

Passaglia, E. & Gottardi, G. (1973): Crystal chemistry and nomenclature of pumpellyites and julgoldites. *Can. Mineral.*, **12**, 219–223.

Robinson, K., Gibbs, G.V., Ribbe, P.H. (1971): Quadratic elongation: a quantitative measure of distortion in coordination polyhedra. *Science*, **172**, 567–570.

Sheldrick, G.M. (1996): SADABS. University of Göttingen, Germany.

— (2008): A short history of SHELX. *Acta Crystallgr. A*, **64**, 112–122.

Yoshiasa, A. & Matsumoto, T. (1985): Crystal structure refinement and crystal chemistry of pumpellyite. *Am. Mineral.*, **70**, 1011–1019.

Received 15 July 2009
Modified version received 22 February 2010
Accepted 9 March 2010